THERMAL MEASUREMENTS ON PENETRATORS: GEOMETRY, SENSITIVITY AND OPTIMISATION ISSUES

A. Hagermann*
S. Tanaka, Y. Saito †

Abstract

The accurate determination of thermal properties is difficult, even in the laboratory, and requires rather complicated experimental setups in most cases. Subsurface measurements of thermal properties as carried out on planetary penetrators are rather restricted by the experimental setup. Among the constraints imposed are (a) a poor control over the nature and orientation of the sample (b) a sometimes unknown thermal contact (c) limited power, time and sampling resolution (d) the geometry of the experiment. These constraints result in experimental designs or procedures that are not optimal for the purpose, so that particular effort needs to be put into the analysis of the measurements. As an example, we discuss the thermal property experiment of the LUNAR–A penetrators. We point out some advantages of the design as well as some of the disadvantages and ways to overcome them.

1 Introduction

When investigating the thermal state of planets (or regions thereof), it is often necessary to investigate the subsurface temperature as a function of depth. Penetrators as vehicles for thermal measurements have been in use for more than five decades now (Hagermann, 2005). Penetrators can play an invaluable role in thermal measurements related to terrestrial heat flow. The ease of deployment is well suited for investigating very small–scale anomalies or inaccessible regions like sea floors. Their easy deployment, compared to the effort of bore–hole measurements, also makes them ideal tools for subsurface thermal investigations of other bodies in the solar system *in situ* (Seiferlin et al., 2001). For our purposes, the planetary subsurface is approximated by a homogeneous and isotropic

* *PSSRI, The Open University, Milton Keynes, U.K.*
† *JAXA–ISAS, Sagamihara, Kanagawa, Japan*

medium of thermal conductivity λ; heat flows in the direction of decreasing temperature ($-\nabla T$). The vector

$$\mathbf{q} = -\lambda \, \nabla T \tag{1}$$

is the heat flux density vector. If we approximate the surface of a terrestrial planet as a homogeneous and isotropic half space, the heat flux density vector – or heat flow – is perpendicular to the surface. Thus, in order to measure planetary heat flow, one needs to measure both λ and the subsurface temperature gradient.

2 In situ determination of planetary subsurface thermal properties

There are many ways to determine λ. Most frequently, the response of the medium under investigation to a known thermal excitation is measured. One can classify these experiments as active methods. There are, however, passive ways of determining the planetary subsurface thermal conductivity at shallow depths, where thermal excitation is provided by the sun, which contributes to the planets' surface energy balances. The solar contribution is periodic because of the planets' rotation and revolution around the Sun. If the surface temperature of a body is subject to a sinoidal temperature variation of amplitude T_0 and period Π, the temperature as a function of time t and depth z takes the form

$$T(z,t) = T_0 \; e^{-z\sqrt{\frac{\pi}{\Pi\kappa}}} \cos\left(\frac{2\pi}{\Pi}t - z\sqrt{\frac{\pi}{\Pi\kappa}}\right) \tag{2}$$

where κ is the thermal diffusivity, i.e. the quotient of λ and heat capacity ϱc.[1] This means that the thermal influence of insolation is attenuated with depth and also experiences a time lag, resulting in a heat wave propagating into the ground. The longer the period of the surface temperature variation, the deeper the surface heat wave will penetrate. The penetration depth

$$z_p = \left(\sqrt{\frac{\pi}{\Pi\kappa}}\right)^{-1} \tag{3}$$

is the depth at which the temperature variation has been damped to $1/e$ of the surface amplitude. On Earth, z_p is usually of the order of several cm for the diurnal heat wave and a few m for the annual heat wave. Equation 1 shows that two parameters need to be measured in order to obtain the heat flow: thermal conductivity λ and temperature gradient $\partial T/\partial z$. Equation (3) shows that at shallow depths, usually in the order of z_p, measurements are likely to reflect external contributions to the surface heat flow, whereas

[1] Strictly speaking ϱc is the specific heat at constant volume, where ϱ is the material density and c the specific heat at constant pressure. Subsequently ϱc is denoted as "heat capacity".

measurements far below the penetration depth z_p usually represent internal contributions. Equation (3) illustrates that λ can be inferred from the thermal penetration depth if heat capacity and density of the planetary sub–surface material are known. Since the heat capacity of regoliths only varies over a relatively small interval compared to thermal conductivity, the estimates obtained by this method can be fairly reliable, as shown by the revision of the Apollo lunar heat flow measurements (Langseth et al., 1972) in the light of long–term observations of subsurface temperature (Langseth et al., 1976). Bullard (1954) used a different, also passive way of determining the thermal conductivity of ocean sediments *in situ*: he estimated the total heat released upon insertion of the heat flow probe/penetrator and derived thermal properties from the cooling curve.

3 Design of thermal property measurement probes

The experimental determination of material thermal properties, mainly of thermal conductivity, has been a topic of measurement science for more than a century now. Many of the methods in use rely on optimal design. Under ideal circumstances, there are methods that permit a measurement of thermal conductivity with an accuracy considerably better than 1%. Among the well–established techniques are the transient line heat source (hot wire) method (Van der Held and Van Drunen, 1949), the guarded hot plate method (Hammerschmidt, 2002) and the divided bar method (Beck, 1957). The analytical and numerical interpretation of these methods has been covered in sufficient detail; the improvement of setup and analysis techniques of the line source, e.g., has been treated in great depth (Bäckström, 1982; Jones, 1988; Takahashi et al., 1994; Banaszkiewicz et al., 1997). However, the design of an optimal experimental setup becomes difficult when designing instruments for space missions. The strict constraints of power, data rate and mechanical robustness often make it impossible to design an optimal experiment. For penetrator experiments, the mechanical constraints are often so harsh that none of the well–established experimental techniques can be used. In addition, thermal contact resistance and small–scale parameters are poorly known. Thermal experiments operating in these conditions represent cases of experimental setups whose design is (and often has to be) sub–optimal. Problems occur where

- there is imperfect thermal contact between sensor components, in particular heaters and temperature sensors,
- there is imperfect thermal contact between the sensor unit and the sample material,
- inhomogeneities in sensor materials occur,
- minor manufacturing faults affect the wiring of the heaters and thermal sensors.

It is fairly obvious that miniaturisation of sensors (as often required within space missions) enhances the above problems.

3.1 Sensors and sensitivity

In addition, the sensitivity of any sensor to the thermal parameters of the sample is dependent upon the geometrical configuration of the experiment and its time constants. The traditional remedy to sub–optimal setup is redesigning the experiment. The transient line heat source (Van der Held and Van Drunen, 1949) can be customised to be very sensitive to thermal conductivity, with a much reduced response to contact resistance and heat capacity of the sample, but its application is limited to samples that permit insertion of, or can be machined to accomodate, a needle–like probe (Von Herzen and Maxwell, 1959). If we aim to employ penetrators as thermal tools, however, the scope for redesign is often close to zero because the thermal experiment is a result of a large number of trade–offs in terms of e.g. geometry, power, size and data rate.

4 The LUNAR–A thermal property measurement

In the case of LUNAR–A, a heated disk of finite radius in a half space is used to estimate thermal conductivity. There are five thermal property sensors on board of each of the Japanese LUNAR–A penetrators, with the aim of investigating the thermal properties of the lunar regolith. The LUNAR–A penetrators, approximately 80 cm long, were designed to impact the surface at a velocity of approximately 300 m/s. The scientific payload of the penetrators comprises seismometers and heat flow experiments. As the determination of the lunar heat flow requires the measurement of the thermal subsurface gradient and thermal conductivity, the LUNAR–A penetrators contain a set of absolute and relative temperature sensors, and also a set of 5 thermal property sensors. The LUNAR–A mission and the heat flow experiment have been described in detail elsewhere (Mizutani et al., 2003; Tanaka et al., 1999). Technically, the LUNAR–A disk heater method is related to the transient plane heat source technique (Gustafsson, 1991; Karawaki and Suleiman, 1991, Nagai et al., 2000). The thermal property sensors consist of a copper disk embedded in an epoxy–microballoon potting. Below the copper disk, there is a sheet heater and a thermocouple temperature sensor. During operation, a constant power of 50 mW is supplied to the sheet heater for 2 minutes. Temperature is sampled at 16 Hz during the heating process and afterwards for a total duration of 4 minutes. During qualification and calibration, a sampling frequency of f =20 Hz was used. The response of the system to heating should depend on the thermal properties of the materials: the thermal properties of the materials on one side of the heated plate are well known, because these compose the penetrator; the adjacent half space is filled by the lunar regolith (or, on Earth, some other sample material) whose properties are to be investigated. In principle, this method can be approximated by a disk heater at the boundary between two half spaces, and an analytical solution that describes the increase of temperature with time can be found (Carslaw and Jäger, 1959). Based on this analytical solution, Horai et al. (1991) have developed an analytical method for finding the thermal inertia of the sample material using the initial slope of the temperature curve. A discussion of the strengths and shortcomings of their method is beyond the scope of this study.

In order to investigate the characteristics of the experiment, we have constructed a thermal

mathematical model (TMM) of the sensors. Given their simple, cylindrical geometry (see Figure 1, an implicit control volume method is a very suitable approach. Our model consists of 14 radial and 19 vertical cells. Because of the small size of the sensors, physical properties of the sensor components could not be measured directly. Subsequently they were taken from datasheets or measurements of sufficiently large analogue samples. We used experimental data for three of our sensors using a variety of sample materials. The reference materials were styrofoam (MC1), rubber (MC2) and glass (MC3) calibrants supplied by Showa Denko Ltd. Their thermal conductivities were given as 0.036, 0.244 and 1.398 W/m/K respectively. Thermal conductivity can safely be assumed to be constant over the temperature range of our measurements. The parameter space spans two orders of magnitude and any method that gives the thermal conductivity reliably and reproducibly within 30% accuracy for all of our sensors and all materials we consider as sufficiently accurate for our purposes.

Once a suitable correction for the heat loss through the wires has been found, the heating curve of the calibration experiments can be reproduced by the TMM with satisfactory accuracy (the meaning of the word 'satisfactory' in this context will be discussed later). Numerical models can, of course, only be imperfect reproductions of the true system. We chose not to include the thermal contact resistance in our models because this quantity is poorly known and hardly reproducible.

We calibrated a set of nominally identical sensors using the same sample material and heating power. The recorded temperature response to heating varied considerably (sometimes several K) between the sensors. As the sensors are small in size and manufactured from virtually identical parts, this mismatch can mainly be explained by small–scale diversions from the nominal model, the most important of which is thermal contact resistance. Most of these small–scale effects only influence the temperature increase at short ($t < 1$ s) timescales, but the difference in temperature increase at early times has a knock–on effect on the temperatures at later times throughout the heating and cooling process. One additional complication introduced by these small–scale effects is the fact that they also affect the analytical solution by Horai et al. (1991), because they are most dominant at times where this solution is valid, namely short timescales.

The importance of the respective small–scale effects depends on the sample material. Thermal conductivity of good thermal conductors tends to be underestimated because of the thermal contact resistance between the heat source and the sample. Poor thermal conductors are affected by heat escape through the wires, which leads to a slower temperature increase. It is therefore extremely difficult to generate a TMM that is valid for samples over a large range of thermal conductivities.

Experiments with a sample calibrant (MC2) using nominally identical sensors (see Figure 2) illustrate that reproducibility critically depends on absolutely identical experimental conditions, a requirement that cannot be met outside the laboratory. The curve with the lowest temperature increase is (quite obviously) our TMM which does not include an estimate of the thermal contact resistance between copper disk and sample material. The difference between the model curves and the measured curves is comparable with the variation between the measured curves. This is what we understand by a satisfactory agreement of measured and calculated temperatures, accurate enough for most practical

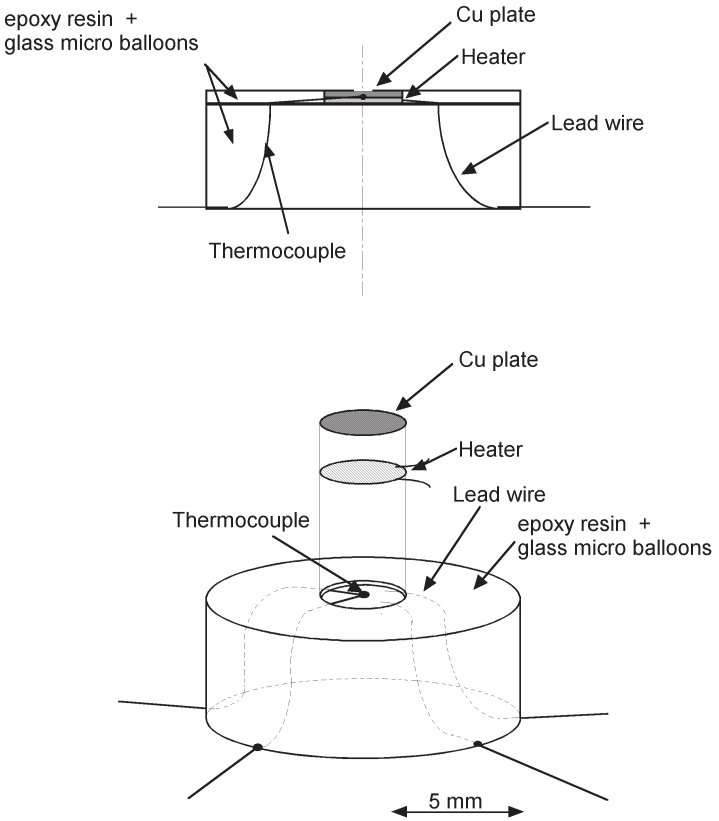

Figure 1: LUNAR–A thermal property sensor.

purposes. Further experiments indicate that the temperature increase depends on the load on top of the sample, meaning that the thermal conductivity measurement is strongly influenced by thermal contact resistance, which cannot be controlled. One might argue that a contact resistance could have been included in the TMM. Since the precise value is not known, it could only be introduced into the model as an additional free parameter. Our numerical tests of the method, however, showed that this additional degree of freedom negatively affected the robustness of the method.

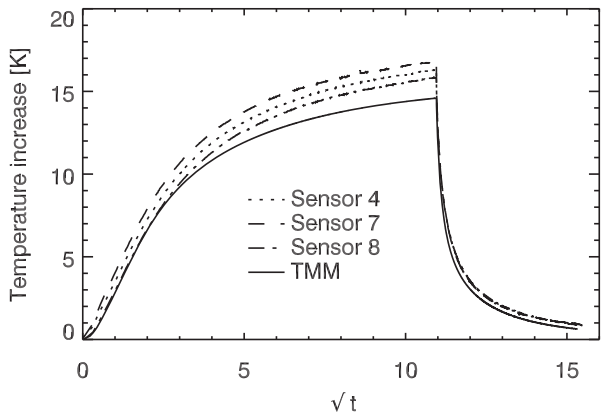

Figure 2: Heating curves of three thermal property sensors using the same calibration material (MC2) and a model prediction curve. The TMM profile is almost indistinguishable from the recorded curves, thermal contact resistance causes the model temperature increase to be lowest.

4.1 Recovery of thermal properties

Derivation of the properties of a sample from the response of the sample to thermal changes can be regarded as a special case of a parameter estimation problem, namely an *Inverse Determination Heat Conduction Problem* (IDHCP). We distort the thermal equilibrium of a medium of unknown thermal conductivity λ, e.g. by supplying heat at a known rate over a known region. In the medium we have a temperature sensor which measures the temperature $U(t)$ at times $t_j, j = 0, 1, 2, \ldots k$. We also have a TMM of the system. The temperatures at the measurement locations calculated by our model $V(t)$ depend on the assumed thermal conductivity λ. The thermal properties of the model are now adjusted such that the residual between observed and measured temperatures is minimal. This is achieved by minimizing the functional

$$J(\lambda) = \int_{t_0}^{t_k} [U(t) - V(\lambda, t)]^2 \, dt \tag{4}$$

A general treatment of this type of inverse problems has been presented by Jarny et al. (1991), more specific solutions can also be found in the literature (Tervola, 1989; Lesnic et al., 1996; Zhan and Murio, 1998). In this particular experiment, the $U(t)$ curve shows a very steep increase in the first few seconds and is almost flat for the rest of the heating pulse. One can substitute

$$x = \begin{array}{ll} \sqrt{t} & \text{for} \quad t \leq t_H \\ \sqrt{t - t_H} & \text{for} \quad t > t_H \end{array} \tag{5}$$

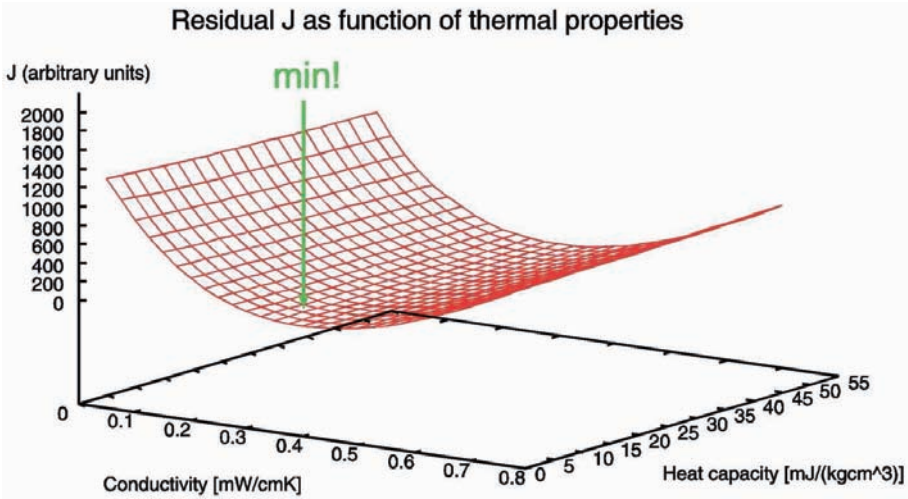

Figure 3: Sensitivity of the LUNAR–A thermal property sensors. The sensitivity plane of residual J is shown as a function of thermal conductivity λ and heat capacity c. The 'λ–valley' constrains thermal conductivity well (here: data for styrofoam), but sensitivity to heat capacity is almost negligible. The green arrow indicates the minimum, i.e. the 'true' thermal characteristics of the sample.

where t_H is the end of the heating pulse, and thus arrive in a parameter space that is convenient for a comparison of the curves, as is illustrated in Figure 2. The IDHCP is a valuable tool for investigating the sensitivity of a thermal measurement to the individual thermal properties of the surrounding material. Figure 3 gives an indication of the sensitivity of a LUNAR–A type experiment to thermal conductivity λ and heat capacity ρc. The J function, which measures the mismatch between modelled and measured temperatures of the experiment, has a very pronounced minimum in λ–space, but in ρc space, the minimum is almost indistinguishable. This indicates high sensitivity of the experiment (and analysis procedure) to thermal conductivity, while heat capacity plays only a very minor role. Consequently, this type of measurement is suitable for planetary heat flow experiments, which require knowledge of λ rather than ρc.

4.2 Application of the IDHCP

One can apply the inverse solution outlined in Equations (4) and (5) to the problem, but the solution is complicated in several ways: Firstly the IDHCP is, by its very nature, an ill–posed problem, meaning that there could be many sets of possible solutions of arbitrary complexity that are able to minimize J. The second difficulty we encounter is methodical: Our experiment design is imperfect in the sense that we only have one single sensor which is located at the same position as the heater, whose thermal coupling with the sample material is not well known. One finds that other experimental setups, e.g.

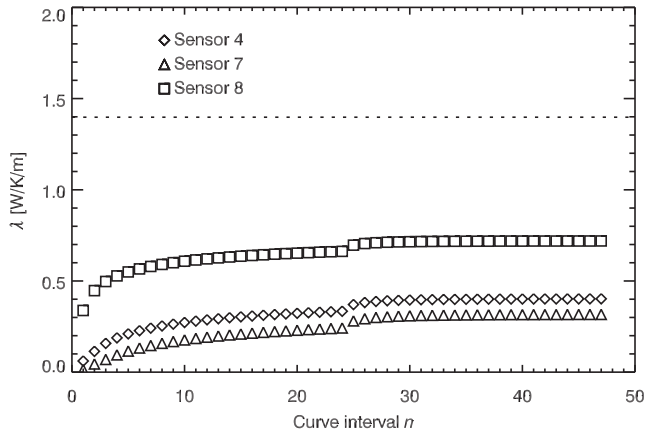

Figure 4: Inverted thermal conductivity values for material MC3 using the classical IDHCP. Note the systematic offset due to (uncontrollable) small–scale effects. The horizontal dashed line indicates the true thermal conductivity.

more sensors, other locations or different geometries of heat sources, will be more suitable for the task of finding thermal conductivity in the sense that the sensitivity of J to the unknown quantity λ is higher. As a consequence, the reproducibility of measurements is limited; a seemingly negligible change of the experiment can result in a completely different thermal conductivity estimate.

4.3 A simple work around

As has been pointed out before, changes on short timescales affect the future increase of the temperature curve, hampering the use of only the later part of the curve for deriving thermal conductivity. We have been looking for ways to reduce this knock–on effect. A practical solution was using the derivative $u(x) = dU/dx$ rather than the $U(x)$ function itself. Derivatives of noisy data are usually dominated by noise in the measurements. Therefore we need a filter process to smooth the temperature curve. A simple, yet effective, filter is a spline fit to the measurements. One can approximate the measurement $U(x)$ using a linear B–spline least squares fit in the x domain. The N spline coefficients a_j are found by minimizing

$$S = \sum_{i=1}^{t_n \times f} \left| U(x_i) - \sum_{j=1}^{N} a_j B_j(x_i) \right|^2 \tag{6}$$

The filtered $u(x)$ then corresponds to the slope of the individual spline sections. The benefits of this kind of spline fit in the x–domain over a fit in the t–domain can be illustrated

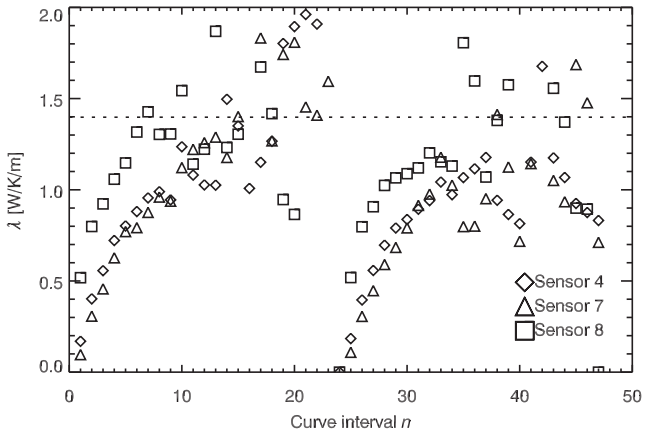

Figure 5: Inverted thermal conductivity values for material MC3 using truncated slopes of a linear spline. Note how systematic offsets are reduced and random errors dominate for $10 < n < 24$ *and* $34 < n < 48$. *True thermal conductivity given by straight, dashed line.*

as follows. At short timescales, when the temperature increase is fast, measurement errors are small compared to the temperature increase, so only few measurements are needed to determine the derivative. At long timescales, when the derivative is more affected by measurement errors because the temperature increases more slowly, more measurements are used to determine the gradient. The number of knots used in the B–spline should depend on the noise level of the measurements; we found 50 knots to be appropriate for a $\sqrt{120\ \mathrm{s}}$ interval. One can now minimize

$$M(\lambda) = \int_{x^{(0)}}^{x^{(1)}} \left(u(x) - \frac{dV(\lambda, x)}{dx} \right)^2 dx \tag{7}$$

where $x^{(n-1)} = \sqrt{t_{n-1} \times f}$ and $x^{(n)} = \sqrt{t_n \times f}$.

The results for our MC3 calibrant are shown in Figure 5. The n parameter determines the section of the linear spline. We can see that the very first data point gives a good estimate of the thermal conductivity approximately for $10 < n < 24$ and $34 < n$. Note values with low n are essentially derived from the starting slope of the temperature increase and are therefore to some extent comparable to what would be obtained using Horai et al.'s method without prior assumptions or corrections.

λ values derived from the early part of the heating curve underestimate (or, in case of a sample of low thermal conductivity, overestimate) the true thermal conductivity due to the effects mentioned in Section 4.1. The estimate improves (i.e. the λ–value increases) as n increases because the short–timescale response of the system loses importance. This behaviour is repeated during the cooling process (i.e. $n > 24$). Averaging the values over

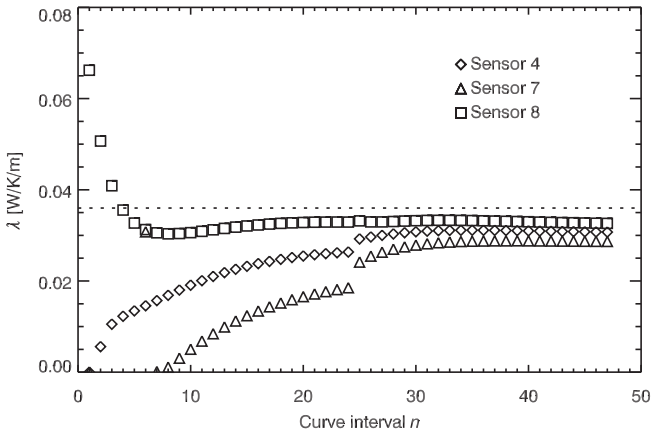

Figure 6: Inverted thermal conductivity values for material MC1 using the classical IDHCP. The systematic error due to small–scale effects has become smaller compared to the low–conductivity MC3 calibrant. Also note how thermal conductivity is now overestimated at the start of the heating cycle of sensor no. 8.

various sections of the curve could improve our estimate. As the start of the heating curve is known to be dominated by small–scale effects, we can start averaging at a later point, but an unambiguous way of determining a suitable time interval still has to be found.

5 Experimental results

In order to assess the benefit of using truncated slopes we compare the thermal conductivity estimates with those returned by the IDHCP. We have solved the IDHCP using a procedure as described in Equation 4 and investigated the effect of the choice of cut–off point t_n on the parameters by dividing the time axis space into intervals, facilitating comparison with the results obtained by using the spline fit. Again, our subdivision means that all calculations for $n > 24$, i.e. $t_n > 120$ s, take into account not only the heating, but also the cooling curve. We present the results for the MC3 and MC1 calibrants. The results shown in Figure 4 indicate that the value of thermal conductivity obtained by the IDHCP procedure not only depends on the choice of t_n; in all experiments, the thermal conductivity of the sample is also systematically underestimated. Using the derivative fitting procedure with splines outlined above (Figure 5), the estimated λ value during the first part of the heating/cooling curve also strongly depends on the time of the estimate. However, approximately $n = 10$ steps into the heating/cooling cycle, random errors dominate. The systematic offset is much reduced in these sections, compared to the IDCHP. Results of both procedures with calibrant MC1, a much poorer conductor than MC3, are shown in Figures 6 and 7 respectively. When applied for a complete heating/cooling cy-

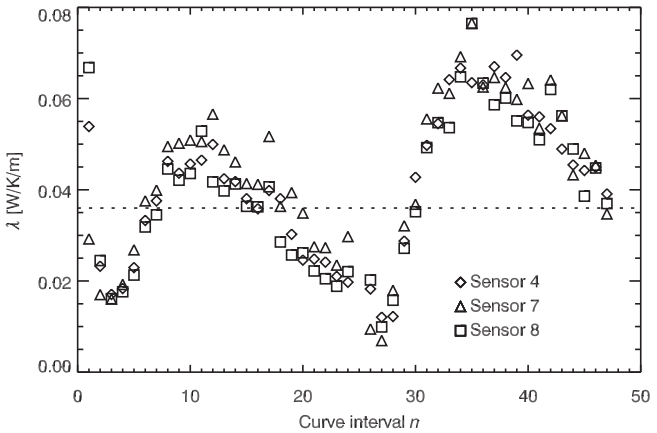

Figure 7: Inverted thermal conductivity values for material MC1 using the slopes of a linear spline. After the initial heating period, systematic errors play a role, but their magnitude is dependent on the progress of the heating cycle.

cle, the IDHCP gives good results, although a minor systematic, sensor–dependent, offset remains. The slope–based fitting procedure exhibits larger scatter and is more time–dependent in this case. Averaging over certain time intervals would reduce errors. The variation of the discrepancy between true λ and the estimated value as a function follows a systematic pattern which has to be further investigated.

6 What have we learnt?

We have presented the characteristics of active thermal conductivity measurements operating in severely constrained conditions. The case of the LUNAR–A thermal property sensor served as an example to indicate some of the challenges and opportunities for data analysis. We compared the usage of the IDHCP with a method that uses time derivatives using a linear spline as a filter. Our results indicate that it seems to be possible to trade off the systematic errors associated with the IDHCP solution for higher random errors, which appears counter–intuitive. We have apparently reduced the sensitivity to contact resistance effects, which seems due to the fact that our method focuses on the latter part of the heating curve. Our interpretation is that, by using the slope of the curve, the impact of the first moments of heating is reduced; since we are dealing with a diffusion problem, the solution is more sensitive to small–scale effects at short timescales. Using the IDHCP requires use of the full heating curve, thus making it impossible to ignore the temperature increase of the first moments of heating (which affects the amplitude of the complete temperature increase). By using a time derivative, we seem to be able to subdue the influence of the onset of the heating on the remaining curve. The dominance

of random versus systematic errors observed in our tests need not necessarily be a drawback; the impact of random errors can be reduced by averaging. However, we believe that more work is needed to fully understand our findings and possibly improve the method of analysis. Ultimately we think that, for a material of entirely unknown thermal properties, a combination of both methods will give reliable results, even if the experimental setup is not optimal.

Acknowledgments

This paper is a contribution to the 2^{nd} *International Workshop on Penetrometry in the Solar System*. The authors would like to thank its organisers at the IWF Graz. A.H. acknowledges financial support from the European Commission (project 001637). Some of the activities reported in this paper were funded by JSPS, the Alexander–von–Humboldt Foundation and Monbukagakusho. All authors wish to express their gratitude to Hitoshi Mizutani for his continued support and guidance.

References

Bäckström G.: Determination of thermal properties using a shielded thermocouple. *J. Phys. Sci. Instrum.* **15**, 1049–1053 (1982).

Banaszkiewicz M., Seiferlin K., Spohn T., Kargl G., Kömle N.I.: A new method for the determination of thermal conductivity and thermal diffusivity from linear heat source measurements. *Rev. Sci. Instrum.* **68**, 4184–4190 (1997).

Beck A.E.: A steady state method for the rapid measurement of the thermal conductivity of rocks. *J. Sci. Instr.* **34**, 186–189 (1957).

Bullard E.: The flow of heat through the floor of the Atlantic Ocean. *Proc. Roy. Soc. London A* **222**, 408–429 (1954).

Carslaw H., Jäger J.: *Conduction of Heat in Solids*. 2^{nd} Edition. Clarendon Press, Oxford (1959).

Gustafsson S.E.: Transient plane source techniques for thermal conductivity and thermal diffusivity measurements of solid materials. *Rev. Sci. Instrum.* **62**, 797–804 (1991).

Hagermann A.: Planetary heat flow measurements. *Phil. Trans. Roy. Soc. London A* **363**, 2777–2792 (2005).

Hammerschmidt U.: 2002. Guarded hot–plate (ghp) method: Uncertainty assessment. *Int. J. Thermophys.* **23**, 1551–1570 (2002).

Horai K., Fujimura A., Tanaka S., Mizutani H.: Measurement of the lunar regolith thermal conductivity in the LUNAR–A mission. *Lunar Planet. Sci.* **12**, 589–590 (1991).

Jarny Y., Özişik M.N., Bardon J. P.: A general optimization method using adjoint equation for solving multidimensional inverse heat conduction. *Int. J. Heat Mass Transfer* **34**, 2911–2919 (1991).

Jones B.W.: Thermal conductivity probe: development of method and application. *J. Phys E: Sci. Instrum.* **21**, 832–839 (1988).

Karawacki E., Suleiman B.M.: Dynamic plane source technique for simultaneous determination of specific heat, thermal conductivity and thermal diffusivity of metallic samples. *Meas. Sci. Technol.* **2**, 744–750, (1991).

Langseth M., Keihm S., Peters K.:. Revised lunar heat–flow values. In: *Proc. 7th Lunar Sci. Conf.*, pp. 3143–3171 (1976).

Langseth M.G., Clark S.P., Chute J.L., Keihm S.J., Wechsler A.: Heat–flow experiment. In: *Apollo 15 Preliminary Science Report.* NASA–SP 289, Washington, D.C. (1972).

Lesnic D., Elliott L., Ingham D.B.: 1996. Identification of the thermal conductivity and heat capacity in unsteady nonlinear heat conduction problems using the boundary element method. *J. Comput. Phys.* **126**, 410–420 (1996).

Mizutani H., Fujimura A., Tanaka S., Shiraishi H., Nakajima T.: LUNAR–A mission: goals and status. Adv. Space Res. **31**, 2315–2321 (2003).

Nagai H., Nakata Y., Tsurue T., Minagawa H., Kamada K., Gustafsson S.E., Okutani T., 2000. Thermal conductivity measurement of molten silicon by a hot–disk method in short–duration microgravity enviroments. *Japan. J. Appl. Phys.* **39**, 1405–1408 (2000).

Seiferlin K., Hagermann A., Banaszkiewicz M., Spohn T.: Penetrators as tools for thermal measurements: the MUPUS case. In: Kömle N.I., Kargl G., Ball A.J., Lorenz R.D. (Eds.), *Penetrometry in the Solar System*, pp. 161–184, Verlag der Österreichischen Akademie der Wissenschaften, Vienna (2001).

Takahashi H., Hiki Y., Kogure Y.: An improved transient hot–wire method for studying thermal transport in condensed matter. *Rev. Sci. Instrum.* **65**, 2901–2907 (1994).

Tanaka S., Yoshida S., Hayakawa M., Fujimura A., Mizutani H.: Development of the heat flow measurement system by the LUNAR–A penetrators. *Adv. Space Res.* **23**, 1825–1828 (1999).

Tervola P.: A method to determine the thermal conductivity from measured temperature profiles. *Int. J. Heat Mass Transfer* **32**, 1425–1430 (1989).

Van der Held E.F.M., Van Drunen F.G.: A method of measuring the thermal conductivity of liquids. *Physica* **15**, 865–881 (1949).

Von Herzen R., Maxwell A.E.: The measurement of thermal conductivity of deep–sea sediments by a needle–probe method. *J. Geophys. Res.* **64**, 1557–1563 (1959).

Zhan S., Murio D.A.: Identification of parameters in one–dimensional IHCP. *Computers Math. Appl.* **35**(3), 1–16 (1998).